


FULL PAPER

Open Access



Tiangong-1's accelerated self-spin before reentry

Hou-Yuan Lin^{1,6}, Ting-Lei Zhu^{1,6}, Zhi-Peng Liang^{2,6}, Chang-Yin Zhao^{1,6*} , Dong Wei^{1,6}, Wei Zhang^{1,6}, Xing-Wei Han^{2,6}, Hai-Feng Zhang^{3,6}, Zhi-Bin Wei⁴, Yu-Qiang Li^{5,6}, Jian-Ning Xiong^{1,6}, Jin-Wei Zhan^{1,6}, Chen Zhang^{1,6}, Yi-Ding Ping^{1,6}, Qing-Li Song^{2,6}, Hai-Tao Zhang^{2,6} and Hua-Rong Deng^{3,6}

Abstract

The detection and study of the rotational motion of space debris, which is affected by environmental factors, is a popular topic. However, relevant research in extremely low-orbit regions cannot be conducted due to a lack of observational data. Here, we fill in the gaps to present the rotational evolution of Tiangong-1 in the 5 months prior to reentry. Derived from the changes in the relative distance of its two corner cube reflectors from satellite laser ranging data, the angular momentum of Tiangong-1, which is relatively stable during observation, deviates from its maximum principal axis of inertia and precesses around the normal direction of the orbital plane due to gravity gradient torque at an angle of $23.1^\circ \pm 2.5^\circ$. Requiring consistency with the relationship between the angular momentum and precession rate leads to a solution for the rotation rate, which is thus found to increase. This result cannot be explained by any previously developed torque models. Hence, an atmospheric density gradient torque (ADGT) model that considers the torque generated by the change in atmospheric density with orbital altitude at the satellite scale is proposed to explain the rotational acceleration mechanism of extremely low-orbit objects. The numerical results show that the ADGT model provides a non-negligible ability to explain, but cannot fully describe, the acceleration effect. The data on the rotational evolution of Tiangong-1 can provide an important basis for aerodynamic model improvement by addressing minor factors omitted in previous models.

Keywords: Tiangong-1, Rotational state estimation, Space debris, SLR

Introduction

When the fourth artificial satellite in human history, Vanguard I, was launched in 1958, its rotational speed was found to decay exponentially with time, which was suggested to be the effect of eddy current torque (Wilson 1959; LaPaz and Wilson 1960). After decades of research, eddy current torque has been verified as the main dissipation factor that causes a decrease in spacecraft rotational speed (Smith 1962; Williams and Meadows 1978; Praly et al. 2012; Lin and Zhao 2015). However, some observations of individual rockets show that they have increasing rotational speed (Meeus 1971), and some satellites begin to spin after losing attitude control.

The causes of accelerated spin have not been clearly explained. Whether these phenomena are due to satellite fuel leaks (Boehnhardt et al. 1989), accidental collisions, or the continuous action of certain factors in space cannot be confirmed from scattered observations.

In recent years, the task of active debris removal has spurred the need for the detection of and research on the rotational state of space debris (Liou and Johnson 2009; Liou 2011; Bonnal et al. 2013; Deluca et al. 2013; Shan et al. 2016). Estimating the rotational state of space debris is very difficult when using ground-based observations because of the limited detection capability and the small amount of acquired data. The existing detection and research results are limited to objects at orbital altitudes of approximately 500–1500 km or higher, and such objects are relatively easy to detect (Kucharski et al. 2013; Koshkin et al. 2016; Lin and Zhao 2018; Pittet et al. 2018). In the extremely low-orbit region (altitudes lower than

*Correspondence: cyzhao@pmo.ac.cn

¹ Purple Mountain Observatory, Chinese Academy of Sciences, Nanjing 210034, China

Full list of author information is available at the end of the article

300 km), the small number of detectable objects coupled with their high velocity, short pass duration, and short orbital lifetime require better observation conditions and higher observation capability. To date, comprehensive data on the rotational evolution of extremely low-orbit objects are unavailable, and the high-profile Tiangong-1 reentry event provided an excellent opportunity for data collection.

Tiangong-1, China's first prototype space station, was launched in September 2011. After its service ended in March 2016, its orbital altitude gradually decreased, and the satellite reentered the atmosphere on April 2, 2018, at UTC 0:15. Tiangong-1 was equipped with two corner cube reflectors (CCR), which can be used for satellite laser ranging (SLR), on the docking interface (Fig. 1). The SLR technique measures the round-trip time of laser pulses from the observatory to the satellite to calculate distance (Pearlman et al. 2002). Modern SLR systems can provide instantaneous range measurements at centimeter-level precision, or even millimeter level for single shot, making these systems the most precise technique to track spacecraft in low Earth orbits (Tapley et al. 2004). We organized an optical and laser joint observation of Tiangong-1 from November 2017 (at an altitude lower than 300 km) to March 2018 and obtained 95 passes of

SLR data, of which 40 passes can be used to estimate the rotational state of the satellite. By processing these data in combination with the dynamic model (Lin et al. 2016) and the relationship of all effective solutions, we obtain the rotational state of Tiangong-1 as well as the evolution thereof in the 5 months prior to reentry and fill in the gaps in the rotational evolution data on extremely low-orbit objects.

Methods

Processing of SLR data

The rotational state of Tiangong-1 can be determined by the changes in the relative distance ΔP of its two CCRs (Fig. 2). This change in distance is due to the combined effect of changes in the observation direction and the satellite attitude. As the larger CCR has multiple reflectors, the relative distance obtained is not necessarily the distance between the centers of the two CCRs. Hence, an additional distance factor δp , which is within ± 0.15 m according to its size, is added to the calculation (see Eq. (3)) to correct the distance deviation. In addition, due to the limitations of the observation conditions, the data signals from the small CCR are not evenly distributed (Fig. 2), and the weights of the data need to be adjusted to ensure calculation accuracy.

Estimation of the orientation of angular momentum

The inertia ellipsoid of a rigid body can be established in the body-fixed coordinate system based on the principal moment of inertia I_x, I_y, I_z (Markeyev 2006), as shown in Fig. 3. For a general case of torque-free rotational motion, the angular momentum and angular velocity (instantaneous rotational axis) on the inertia ellipsoid are not constants. The trajectory of the angular velocity is called the polhode. Define $L = H^2/2EI_z$, where H and E are the angular momentum magnitude and the kinetic

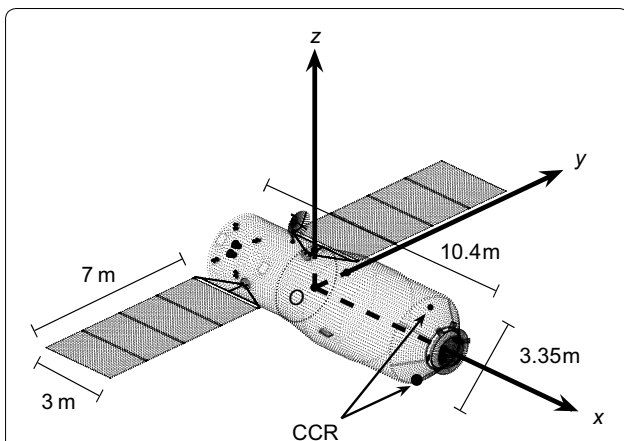


Fig. 1 Model of Tiangong-1 and its body-fixed coordinate system. The main body of Tiangong-1 is 10.4 m in length with a maximum diameter of 3.35 m and a weight of 8.5 t. The two solar panels on either side of the satellite have dimensions of 7 m x 3 m. A body-fixed coordinate system is established with the center of mass of the model as the origin O. The three coordinate axes are along the principal axes of inertia, where the Ox-axis points along the minimum axis of inertia in the docking direction and the Oz-axis follows the maximum axis of inertia. The principal moments of inertia are $I_x = 16,403.01 \text{ kg m}^2$, $I_y = 70,915.56 \text{ kg m}^2$, and $I_z = 76,392.38 \text{ kg m}^2$. The relative vector of the centers of the two corner cube reflectors on the docking interface (from the large one to the small one) can be expressed in the body-fixed coordinate system as $P_0 = (-0.2029, 0.6406, 2.6625) \text{ m}$

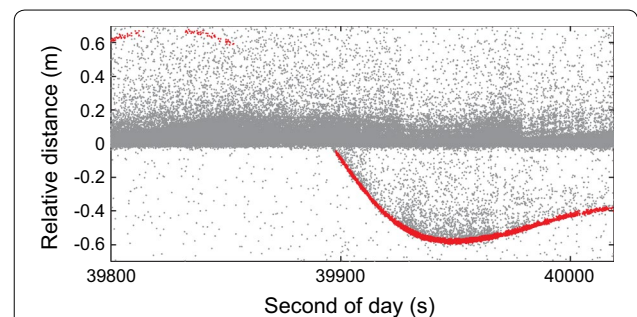
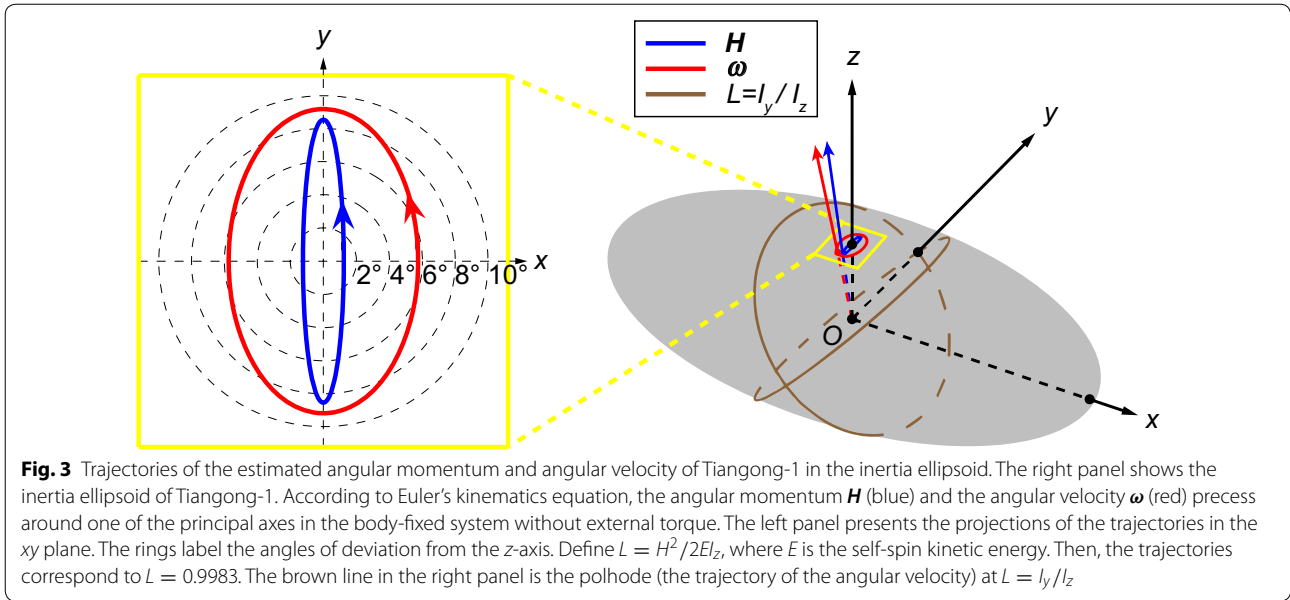


Fig. 2 Example of SLR data of Tiangong-1 on January 18, 2018, at UTC 11.1 h. The abscissa is the second of day, and the ordinate is the relative distance from the large CCR to the small CCR. The gray data are measured from the large CCR with background noise. The red marks the signals from the small CCR



energy of self-spin, respectively. Then, L can indicate the position of the trajectory of the angular velocity and the angular momentum in the inertia ellipsoid. The polhode when $L = I_y/I_z$ (the brown line in Fig. 3) divides the inertia ellipsoid into four regions (Markeyev 2006), in which the polhode surrounds $\pm x$ or $\pm z$. When L is equal to 1 and I_x/I_z , the axes of rotation coincide with the Oz - and Ox -axes, respectively. Because the magnitude of angular velocity is not constant in a polhode, when comparing the rotational speeds at different times, the equivalent rotational speed H/I_z can be used to characterize the change in rotational speed due to external torque.

On the basis of the rotational motion model with 6 main parameters $H, \psi_H, \theta_H, \varphi_H, \theta',$ and φ' (Lin et al. 2016; Crenshaw and Fitzpatrick 1968) shown in Fig. 4, we can establish the transformation between the body-fixed coordinate system and the orbital plane coordinate system. Define $\mathbf{R}_\xi(\eta)$ as a rotation matrix around axis ξ with angle η . Then, the transformation matrix from the orbital plane coordinate system to the body-fixed system can be written as

$$\mathbf{T}_{ob} = \mathbf{R}_{Oz}(\varphi') \mathbf{R}_{Ox}(\theta') \mathbf{R}_{Oz}(\varphi_H) \mathbf{R}_{On}(\theta_H) \mathbf{R}_{Oz^0}(\psi_H). \tag{1}$$

The numerical test shows that this set of parameters is less sensitive to initial values than other parameter sets (such as the set with the traditional Euler angles and angular velocity vectors), which is beneficial for the calculation. Then, the unit vector to the observation station in the body-fixed system can be expressed as

$$\mathbf{S} = \mathbf{S}(\mathbf{S}_{J2000}, \boldsymbol{\sigma}, H, \psi_H, \theta_H, \varphi_H, \theta', \varphi'), \tag{2}$$

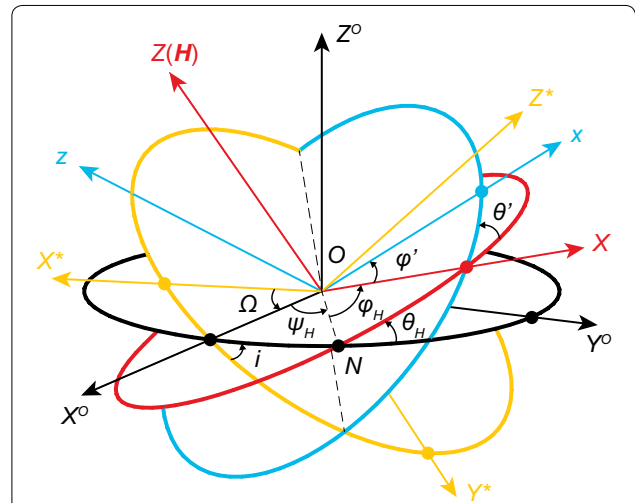


Fig. 4 Coordinate systems and 6 main parameters (Lin et al. 2016). The orientation of the $OX^*Y^*Z^*$ system is fixed in the space. The $OX^0Y^0Z^0$ system is the orbital coordinate system. The $Oxyz$ system is the body-fixed system shown in Fig. 1. The $Oxyz$ system is a system associated with the self-spin angular momentum vector \mathbf{H} . The $Oxyz$ system can be obtained from the $OX^*Y^*Z^*$ system by successive rotations through angles $\Omega, i, \psi_H, \theta_H, \varphi_H, \theta'$ and φ' , where Ω is the longitude of ascending node and i is the orbit inclination

where \mathbf{S}_{J2000} is the unit vector from Tiangong-1 to the observation station in the J2000.0 coordinate system and $\boldsymbol{\sigma}$ are the orbital elements. These values are known variables. Then, the relative distance of the two CCRs in Fig. 2 is written as

$$\Delta P = -\mathbf{S} \cdot (\mathbf{P}_0 + \delta_P), \tag{3}$$

where P_0 shown in Fig. 1 is the relative vector from the center of the large CCR to the small CCR, and δp is the undetermined distance factor to correct the deviation from the centers of the CCRs, as mentioned above. A rotational motion mode can then be obtained using a genetic algorithm that satisfies the changes in ΔP in the observation data.

Usually, multiple possible solutions are obtained for the data from a single pass. Figure 5a shows the solutions for two main parameters, ψ_H and θ_H , which are the spherical coordinates of the self-spin angular momentum H in the orbital plane system. Hence, we need to screen all solutions to eliminate false ones, including inspecting the visibility of the CCRs in the observation geometry (Fig. 5b) and comparing the results from other adjacent passes, i.e., choosing similar values of θ_H and L and conforming the change in ψ_H to the law. This process eventually

yields a certain orientation of the angular momentum (red region in Fig. 5).

Solutions of angular momentum magnitude

Determining the exact angular momentum magnitude H is another challenge. Directly solving the rotational speed is extremely difficult because the valid observation duration in a single pass is much smaller than the rotation period of Tiangong-1, the time interval between adjacent passes is much larger than this rotation period, and the large dimension of the algorithm makes ΔP not sensitive to the changes in H .

However, the direction of the angular momentum (ψ_H, θ_H) can be accurately determined in a single pass, and the solution in each pass is a mutually independent process (Fig. 6). Due to the influence of the gravity gradient torque, the angular momentum precesses around the normal of the orbital plane. Variations in ψ_H can be reduced to a first-order secular linear change and a second-order periodic change (Lin et al. 2016). For a triaxial ellipsoid model, the linear change rate of ψ_H can be approximated as

$$\begin{aligned} \omega_{\psi_H} = & -\cos i \cdot \dot{\Omega} \\ & + \frac{3GM}{4R^3H} \cos \bar{\theta}_H (I_x(1 - 3 \sin^2 \bar{\theta}' \sin^2 \bar{\varphi}') \\ & + I_y(1 - 3 \sin^2 \bar{\theta}' \cos^2 \bar{\varphi}') + I_z(1 - 3 \cos^2 \bar{\theta}')), \end{aligned} \tag{4}$$

where i is the orbit inclination, $\dot{\Omega}$ is the orbital precession caused by the oblateness of the Earth, G is the gravitational constant, M is the mass of the Earth, R is the geocentric radius, and $\bar{\theta}_H, \bar{\theta}'$, and $\bar{\varphi}'$ are the mean values of θ_H, θ' , and φ' , respectively (Lin et al. 2016). The first-order linear change rate of ψ_H is approximately linear with $1/H$. This correspondence is easy to understand because the gravity gradient torque is independent of the angular momentum, and under the same gravity gradient torque effects, the smaller the magnitude of the angular momentum is, the more easily the direction is changed, which results in a faster change rate.

Therefore, the magnitude of the current angular momentum H can be obtained from the change in ψ_H from two passes based on the relationship between H and the precession rate of the angular momentum. In actual operation, the resulting error will be excessive if the two passes are too close, and if their time interval is too long, the large difference in orbital altitudes will affect the $\psi_H - H$ relationship. Therefore, we select the interval from the observations to be more than half a day and less than 10 days to calculate the change in ψ_H . After eliminating the incorrect solutions for the difference angles of ψ_H in the same quadrant, the magnitude of the angular

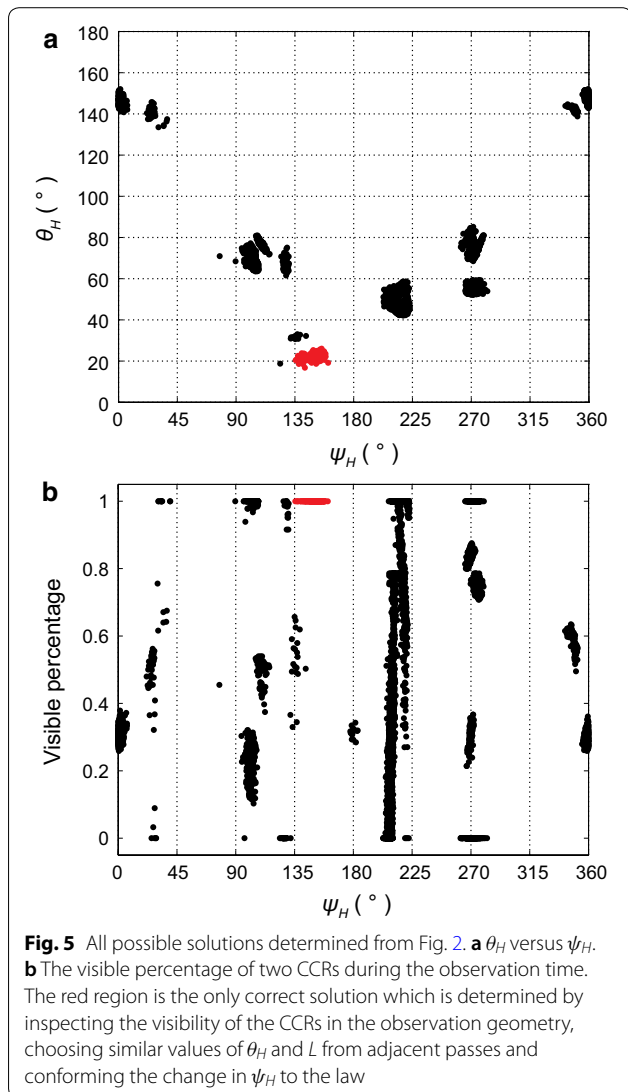


Fig. 5 All possible solutions determined from Fig. 2. **a** θ_H versus ψ_H . **b** The visible percentage of two CCRs during the observation time. The red region is the only correct solution which is determined by inspecting the visibility of the CCRs in the observation geometry, choosing similar values of θ_H and L from adjacent passes and conforming the change in ψ_H to the law

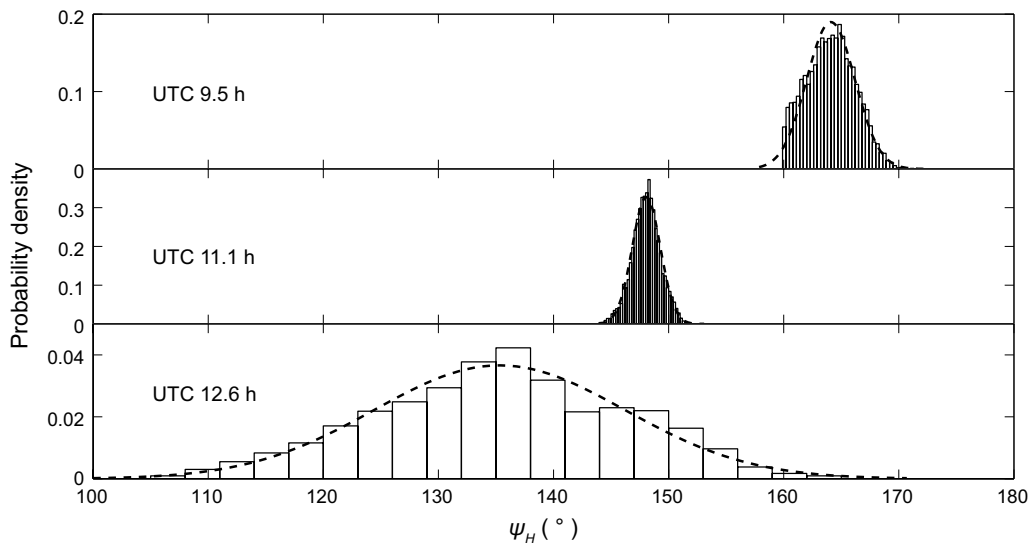


Fig. 6 Probability distributions of the estimated ψ_H . The three sets of data are estimated from three consecutive passes on January 18, 2018, at UTC 9.5 h, 11.1 h, and 12.6 h. Due to the influence of the gravity gradient torque, ψ_H will increase or decrease at a certain rate, which can be used to find the correct solution in Fig. 5 and calculate the magnitude of the angular momentum in Fig. 7

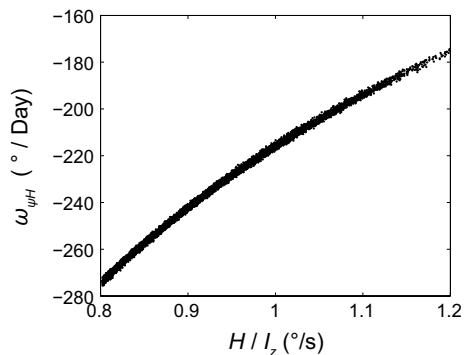


Fig. 7 Relation between the change rate of ψ_H and the equivalent rotation speed H/I_z . The relation example is estimated from Fig. 2 where the orbit altitude is approximately 280 km. A series of parameter sets of rotational motion, which are not sensitive to H , are obtained using Eq. (3). We use each set of parameters as initial values to extrapolate the rotation and extract the change rate of ψ_H . Then, we can establish a mapping from H/I_z to ω_{ψ_H} . Once the change in ψ_H from two passes is determined, the exact H/I_z can be reversed

momentum can be obtained by numerically calculating the ψ_H – H relationship (Fig. 7).

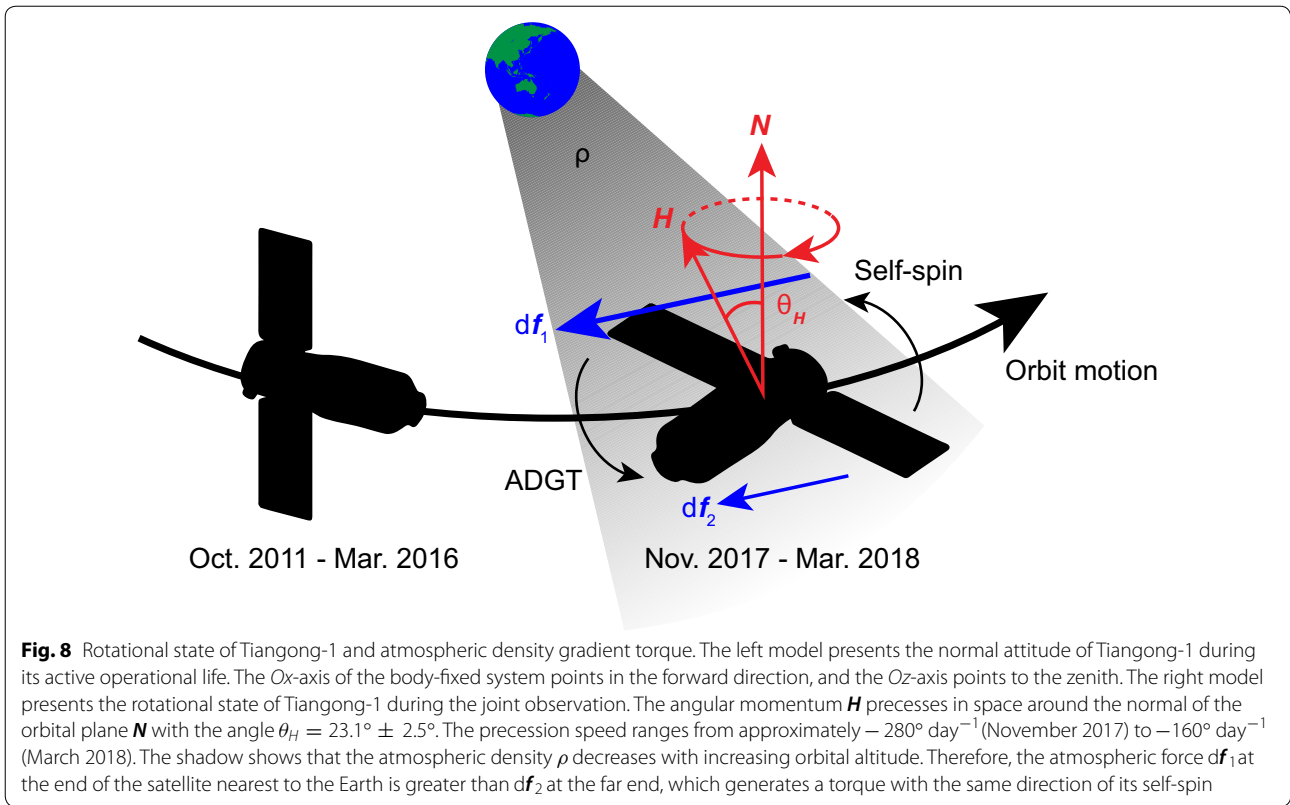
Results and discussion

Tiangong-1’s rotational state

The evolution of the rotational state of Tiangong-1 can be expressed by the variation of its self-spin angular momentum because the angular momentum is the conserved quantity in the rotational motion of a rigid body

without external torque. Derived from the estimation results, the angular momentum H of Tiangong-1 deviates from its z -axis (i.e., the maximum principal axis of inertia) with maximum angles of approximately 1° and 8.5° in the x and y directions, respectively (Fig. 3), while in the inertial space, the angular momentum H precesses around the normal direction N of the orbital plane due to gravity gradient torque (Lin et al. 2016) at an angle $\theta_H = 23.1^\circ \pm 2.5^\circ$ (Fig. 8). During the 5-month observation period, the rotation mode of Tiangong-1 was relatively stable, indicating that the satellite was not subjected to a strong sudden effect (such as a collision). Any dissipating effect in space will cause the angular momentum to migrate to the axis of maximum inertia (the rotation with the lowest energy), but Tiangong-1’s angular momentum remained at a certain angle to the z -axis for a long duration. A numerical test showed that gravity gradient torque produces only periodic deviations of up to 0.01° (along the x -axis) and 0.1° (along the y -axis). Therefore, we speculate that Tiangong-1 was also subject to other effects, which may be additional stable driving torques. Combined with the attitude of Tiangong-1 before losing attitude control (Fig. 8), these effects may have caused the Oz -axis to be deflected by approximately 90° in the normal direction of the orbit plane, finally reaching a balanced state.

An accurate magnitude of the angular momentum H can be derived through the relationship of H with the precession rate of the angular momentum due to the gravity gradient torque, thus enabling the



variation in rotational speed with time to be obtained (Fig. 9). The rotational speed of Tiangong-1 increased in the 5 months before reentry. This acceleration phenomenon has been verified by a very small amount of imaging and radar data. Although a complete period evolution cannot be obtained from these additional data, the detected rotational speed in early 2018 is clearly faster than that at the end of 2017. As mentioned in Introduction, this difference is an unexpected phenomenon. Within the known major external torques in space, the gravity gradient torque generally acts as a conservative torque and does not have a secular effect on the angular momentum (Lin et al. 2016; Crenshaw and Fitzpatrick 1968; Holland and Sperling 1969; Hitzl and Breakwell 1971). The eddy current torque and magnetic torque are dissipative torques that decrease the rotational speed (Smith 1962; Williams and Meadows 1978; Praly et al. 2012; Lin and Zhao 2015). Light pressure torque may theoretically have a slight acceleration effect under specific orbit and attitude configurations (Kucharski et al. 2016), but no secular effect was found in our numerical test on Tiangong-1. Classic aerodynamic torque, which affects objects only at very low orbital altitudes (Williams and Meadows 1978; Lyle and Stabekis 1971; Hart et al. 2014), will also decrease rotational speed (blue line in Fig. 9).

Atmospheric density gradient torque

However, we conjecture that the upper atmosphere is the factor causing the increase in the rotational speed because the acceleration of the spin increases significantly with decreasing orbital altitude, which is consistent with the increase in atmospheric density with decreasing orbital altitude. In this regard, we propose an atmospheric density gradient torque (ADGT) model (Fig. 8), which takes into account the torque generated by the change in atmospheric density with orbital altitude at the satellite scale. For the rotational state of Tiangong-1, the ADGT is nearly in the same direction as the angular momentum, resulting in an acceleration effect. The atmospheric density gradient at Tiangong-1's position after February 2018 also increases faster (upper panel of Fig. 9), which is consistent with the increasing accelerated rate of the rotational speed.

We can estimate the order of magnitude of this new torque. As shown in Fig. 9, the rotational speed increased by approximately 0.2° s^{-1} from December 1, 2017, to February 1, 2018. Then, the change rate of the angular momentum can be estimated as $\Delta H / \Delta t \sim 5 \times 10^{-6} \text{ kg m}^{-2} \text{ s}^{-2}$. Considering the classic atmospheric force formula, the difference in the forces acting at a distance $L \sim 5 \text{ m}$ is

$$\Delta F = -\frac{1}{2} C_d A v^2 L d\rho \tag{5}$$

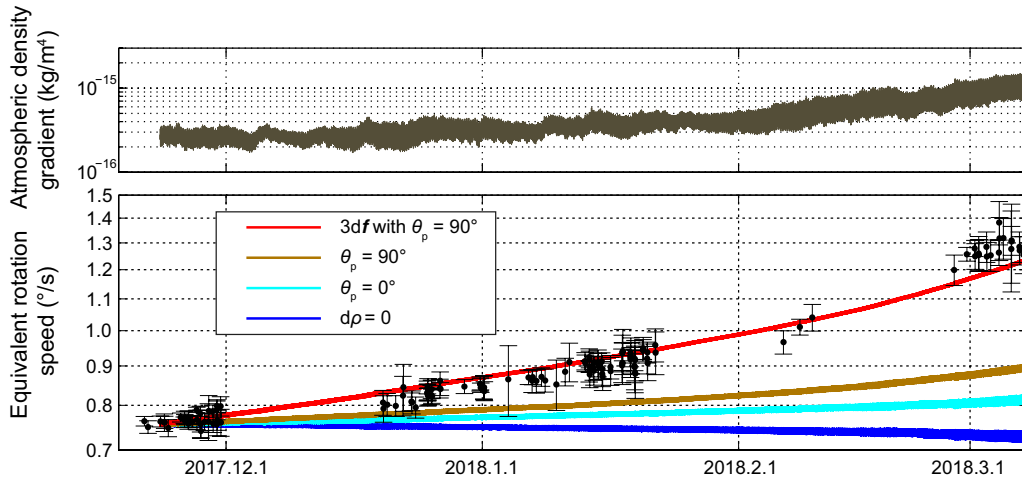


Fig. 9 Variation in equivalent rotational speed (lower panel) and the corresponding atmospheric density gradient (upper panel). The abscissa is the date, and the ordinate is given in logarithmic coordinates. In the upper panel, the atmospheric density gradient (unit: kg m^{-4}) is the gradient of the atmospheric density at the altitude of Tiangong-1's position. The atmospheric density model is MSIS 90, and the orbital and space environment parameters are all actual values. In the lower panel, the black point is the equivalent rotation speed H/I_z (unit: $^\circ \text{s}^{-1}$), which is estimated from the observational data. The error bar marks the range of one standard error. The four curves present the numerically calculated evolutions of the equivalent rotational speed. Each curve has a short-term oscillation with an amplitude of no more than $0.01^\circ/\text{s}$. The blue represents the result for classic aerodynamic torque, and the remaining three lines consider the effect of ADGT, where the cyan and brown lines present the results when the angles θ_p between the normal of the solar panel and the z-axis take values of 0° (flat) and 90° (upright), respectively, and the red shows the results when the atmospheric force $d\mathbf{f}$ acting on the model element is increased threefold when the solar panels are upright. No significant changes in θ_H or L are found in the results, which are comparable to the observational results

where the drag coefficient $C_d \sim 2$, the projected area of satellite normal to the incident flow $A \sim 10 \text{ m}^2$, the velocity of the satellite $v \sim 8 \times 10^3 \text{ m s}^{-1}$, and the gradient of the density in the direction of the orbital altitude $d\rho \sim 3 \times 10^{-16} \text{ kg m}^{-4}$ (taking the value on January 1, 2018 in the upper panel of Fig. 9). Then, the ADGT can be estimated as $T \sim L\Delta F \sim 5 \times 10^{-6} \text{ kg m}^{-2} \text{ s}^{-2}$, which is in line with the increasing rate of the angular momentum.

To verify our ADGT model, we performed a numerical simulation using actual orbital and space environment parameters with aerodynamic torque based on the molecule–surface interaction model (Lyle and Stabekis 1971; Hart et al. 2014) and taking gravity gradient torque into account. The aerodynamic force acting on a unit surface element is

$$d\mathbf{f} = -\rho v^2 \cos \theta_i \left((2 - \sigma_N) \cos \theta_i \hat{\mathbf{n}} - \sigma_T \sin \theta_i \hat{\mathbf{t}} \right) dA, \quad (6)$$

where $\hat{\mathbf{n}}$ is the normal of the surface, $\hat{\mathbf{t}}$ is the tangential vector, θ_i is the incident angle, dA is the area of the unit surface element, and σ_N and σ_T are the normal and tangential momentum exchange coefficients, which both take an empirical value of 0.8 (Lyle and Stabekis 1971). The atmospheric density

$$\rho = \rho_0 + \Delta h \cdot d\rho, \quad (7)$$

where ρ_0 is the atmospheric density at the center of mass and Δh is the altitude difference from the center of mass. The aerodynamic torque is

$$d\mathbf{T} = \mathbf{r} \times (\delta \cdot d\mathbf{f}), \quad (8)$$

where \mathbf{r} is the body-fixed coordinate vector of the unit surface element and δ is the correction coefficient of the force that we add to account for unknown effects.

Normally, δ is set to 1. The acceleration effect of the ADGT, which is independent of rotational speed, overcomes the deceleration effect of classic aerodynamic torque (the brown and cyan lines in Fig. 9). However, a gap exists between the simulation results and the measured data. If we multiply the force from the molecule–surface interaction model by a coefficient $\delta = 3$ in the numerical simulation, we can obtain a result that is similar to the measured data (red line in Fig. 9). Hence, the acceleration effect may have a strong correlation with the atmospheric density gradient, and the ADGT model can be inferred to qualitatively conform to the actual situation. The atmospheric density model used in Fig. 9 is MSIS 90. We have also compared other models such as Ciral1972, DTM1994, and JB2008, and their results are not significantly different.

If we assume that the ADGT model is valid, the atmospheric force acting on Tiangong-1 is larger than that in the molecule–surface interaction model, which indicates

that other effects may be acting on the satellite. Traditionally, the atmosphere on satellite orbits has been treated as being under free molecular flow (Hart et al. 2014), and the density has been regarded as constant at the satellite scale. Here, the density gradient is taken into consideration; thus, the accuracy of the molecular–surface interaction model may not match the accuracy required for modeling weak aerodynamic torques. Further refinements are needed to establish an in-depth atmosphere–surface interaction model. Other minor effects, such as multiple reflection or hydrodynamic effects, that were omitted in classic models should be considered in further research.

Conclusions

By processing Tiangong-1's laser ranging data, we obtained the rotational state in the 5 months before reentry and detected an unexpected increase in rotational speed. Then, we proposed a new torque model ADGT to explain this spin acceleration. Because we are unable to determine the status of solar panels, we performed our simulations for two extreme cases, i.e., the panels are parallel ($\theta_p = 0^\circ$) and perpendicular ($\theta_p = 90^\circ$) to the xy plane, respectively. Although several times weaker than the measured data, the acceleration effect due to the ADGT model is still a non-negligible factor in the increasing angular velocity of Tiangong-1. This effect provides a new explanation for the mechanism of the observed rotation acceleration of extremely low-orbit objects. The data on the rotational evolution of Tiangong-1 obtained during the 5-month-long joint observations will help to improve the relevant models and to promote research on the rotational evolution of extremely low-orbit objects, which has an important impact on the prediction of reentry, satellite attitude control, and the overall active debris removal strategy. More observations of extremely low-altitude debris objects are needed to better understand the cause of the rotational acceleration of Tiangong-1 prior to reentry.

Authors' contributions

HYL and CYZ conceived and designed the study. TLZ and ZPL performed the processing of raw data. DW, WZ, JNX, and JWZ performed orbit determination and scheduled the observation plans. XWH, HFZ, ZBW, YQL, QLS, HTZ, and HRD performed satellite laser ranging and contributed data. CZ and YDP processed the photometry and imaging data for verification. HYL and TLZ wrote the manuscript. All authors read and approved the final manuscript.

Author details

¹ Purple Mountain Observatory, Chinese Academy of Sciences, Nanjing 210034, China. ² Changchun Observatory, National Astronomical Observatories, Chinese Academy of Sciences, Changchun 130117, China. ³ Shanghai Astronomical Observatory, Chinese Academy of Sciences, Shanghai 200030, China. ⁴ Chinese Academy of Surveying and Mapping, Beijing 100830, China. ⁵ Yunnan Observatories, Chinese Academy of Sciences, Kunming 650216, China. ⁶ Key Laboratory of Space Object and Debris Observation, Chinese Academy of Sciences, Nanjing 210034, China.

Acknowledgements

We thank Hong-Bo Wang and Xin Wang for their discussions. We wish to thank the anonymous reviewers for their valuable comments.

Competing interests

The authors declare that they have no competing interests.

Availability of data and materials

The dataset supporting the conclusions of this article is available in the Zenodo repository, <https://doi.org/10.5281/zenodo.1452298>.

Funding

This research was supported by the National Natural Science Foundation of China (Grant Nos. 11533010 and 11703095), the Youth Innovation Promotion Association, CAS (Grant No. 2018353), and the Chinese Academy of Sciences Foundation (Grant No. KGFZD-135-16-012).

Publisher's Note

Springer Nature remains neutral with regard to jurisdictional claims in published maps and institutional affiliations.

Received: 24 October 2018 Accepted: 31 January 2019

Published online: 12 February 2019

References

- Boehnhardt H, Koehnke H, Seidel A (1989) The acceleration and the deceleration of the tumbling period of Rocket Intercosmos 11 during the first two years after launch. *Astrophys Space Sci* 11:297–313
- Bonnal C, Ruault JM, Desjean MC (2013) Active debris removal: recent progress and current trends. *Acta Astronaut* 85:51–60. <https://doi.org/10.1016/j.actaastro.2012.11.009>
- Crenshaw JW, Fitzpatrick PM (1968) Gravity effects on the rotational motion of a uniaxial artificial satellite. *AIAA J* 6(11):2140–2145. <https://doi.org/10.2514/3.4946>
- Deluca LT, Bernelli F, Maggi F, Tadini P, Pardini C, Anselmo L, Grassi M, Pavarin D, Francesconi A, Branz F, Chiesa S, Viola N, Bonnal C, Trushlyakov V, Belokonov I (2013) Active space debris removal by a hybrid propulsion module. *Acta Astronaut* 91:20–33. <https://doi.org/10.1016/j.actastro.2013.04.025>
- Hart KA, Dutta S, Simonis KR, Steinfeldt BA, Braun RD (2014) Analytically-derived aerodynamic force and moment coefficients of resident space objects in free-molecular flow. In: *AIAA SciTech, AIAA atmospheric flight mechanics conference*, National Harbor, MD
- Hitzl D, Breakwell J (1971) Resonant and non-resonant gravity-gradient perturbations of a tumbling tri-axial satellite. *Celest Mech* 3(3):346–383
- Holland RL, Sperling HJ (1969) A first-order theory for the rotational motion of a triaxial rigid body orbiting an oblate primary. *Astron J* 74:490–496. <https://doi.org/10.1086/110826>
- Koshkin N, Korobeynikova E, Shakun L, Strakhova S, Tang ZH (2016) Remote sensing of the Envisat and Cbers-2B satellites rotation around the centre of mass by photometry. *Adv Space Res* 58(3):358–371. <https://doi.org/10.1016/j.asr.2016.04.024>
- Kucharski D, Kirchner G, Lim HC, Koidl F (2013) New results on spin determination of nanosatellite BLITS from high repetition rate SLR data. *Adv Space Res* 51(5):912–916. <https://doi.org/10.1016/j.asr.2012.10.008>
- Kucharski D, Bennett JC, Kirchner G (2016) Laser de-spin maneuver for an active debris removal mission—a realistic scenario for Envisat. In: *Proceedings of the advanced maui optical and space surveillance technologies conference*, Held in Wailea, Maui, Hawaii, 20–23 Sept 2016
- LaPaz L, Wilson RH (1960) Magnetic damping of rotation of the Vanguard I satellite. *Science* 131:355–357
- Lin H-Y, Zhao C-Y (2015) Evolution of the rotational motion of space debris acted upon by eddy current torque. *Astrophys Space Sci* 357(2):167. <https://doi.org/10.1007/s10509-015-2396-2>
- Lin H-Y, Zhao C-Y (2018) An estimation of Envisat's rotational state accounting for the precession of its rotational axis caused by gravity-gradient torque. *Adv Space Res* 61(1):182–188. <https://doi.org/10.1016/j.asr.2017.10.014>

- Lin H-Y, Zhao C-Y, Zhang M-J (2016) Frequency analysis of the non-principal axis rotation of uniaxial space debris in circular orbit subjected to gravity-gradient torque. *Adv Space Res* 57(5):1189–1196. <https://doi.org/10.1016/j.asr.2015.12.036>
- Liou J-C (2011) An active debris removal parametric study for LEO environment remediation. *Adv Space Res* 47(11):1865–1876. <https://doi.org/10.1016/j.asr.2011.02.003>
- Liou J-C, Johnson NL (2009) A sensitivity study of the effectiveness of active debris removal in LEO. *Acta Astronaut* 64(2–3):236–243. <https://doi.org/10.1016/j.actaastro.2008.07.009>
- Lyle R, Stabekis P (1971) Spacecraft aerodynamic torques. In: NASA SP-8058
- Markeyev AP (2006) Theoretical mechanics. Higher Education Press, Beijing
- Meeus J (1971) Satellites artificiels—Observations de périodes photométriques 1968–1971. *Ciel et Terre* 87:606
- Pearlman MR, Degnan JJ, Bosworth JM (2002) The international laser ranging service. *Adv Space Res* 30(2):135–143. [https://doi.org/10.1016/S0273-1177\(02\)00277-6](https://doi.org/10.1016/S0273-1177(02)00277-6). [arXiv:1011.1669v3](https://arxiv.org/abs/1011.1669v3)
- Pittet JN, Šilha J, Schildknecht T (2018) Spin motion determination of the Envisat satellite through laser ranging measurements from a single pass measured by a single station. *Adv Space Res* 61:1121–1131. <https://doi.org/10.1016/j.asr.2017.11.035>
- Praly N, Hillion M, Bonnal C, Laurent-Varin J, Petit N (2012) Study on the eddy current damping of the spin dynamics of space debris from the Ariane launcher upper stages. *Acta Astronaut* 76:145–153. <https://doi.org/10.1016/j.actaastro.2012.03.004>
- Shan M, Guo J, Gill E (2016) Review and comparison of active space debris capturing and removal methods. *Prog Aerosp Sci* 80:18–32. <https://doi.org/10.1016/j.paerosci.2015.11.001>
- Smith G (1962) A theoretical study of the torques induced by a magnetic field on rotating cylinders and spinning thin-wall cones, cone frustums, and general body of revolution. In: NASA eTR R-129
- Tapley BD, Bettadpur S, Watkins M, Reigber C (2004) The gravity recovery and climate experiment: mission overview and early results. *Geophys Res Lett*. <https://doi.org/10.1029/2004GL019920>
- Williams V, Meadows AJ (1978) Eddy current torques, air torques, and the spin decay of cylindrical rocket bodies in orbit. *Planet Space Sci* 26:721–726
- Wilson RH (1959) Magnetic damping of rotation of satellite 1958 β 2. *Science* 130:791–793

Submit your manuscript to a SpringerOpen[®] journal and benefit from:

- Convenient online submission
- Rigorous peer review
- Open access: articles freely available online
- High visibility within the field
- Retaining the copyright to your article

Submit your next manuscript at ► [springeropen.com](https://www.springeropen.com)
